Iterative Learning Control for Soft Landing of Electromechanical Valve Actuator in Camless Engines

Wolfgang Hoffmann, Katherine Peterson, and Anna G. Stefanopoulou

***Abstract*—Variable valve timing allows improvements of internal combustion engines and can be achieved by camless actuation technology. In this paper we consider an electromechanical valve (EMV) actuator. One of the main problems in the EMV actuator is the noise and wear associated with high contact velocities during the closing and opening of the valve. The contact velocity of the actuator parts can be reduced by designing a tracking controller that consists of a linear feedback and a nonsquare iterative learning controller (ILC). With the ILC methodology we update the feedforward signal of the feedback controller every cycle based on the error between the actual valve position and the desired position. The methodology is reviewed and both simulation and experimental results are presented. We explore the disturbance rejection capability of the control scheme by simulating conditions with an unknown force acting on the valve similar to the ones present during varying engine load.**

***Index Terms*—Decoupling, electromechanical systems, engine control, iterative learning control, singular values.**

I. Introduction

VARIOUS studies have shown that optimization of the valve timing of an automotive internal combustion engine results in high fuel efficiency, low emissions and improved torque performance. Because of the potential benefits many automotive engine manufacturers and research laboratories are developing mechanisms that can provide the valve event variability. A promising mechanism is the electromechanical valve (EMV) actuator shown in Fig. 1. It relies on two electromagnets that catch and hold an armature that moves with a damped oscillation between two extreme positions under the forcing of two springs [8]. The control signal to the electromechanical actuator is the voltage applied to either one of the coils of the two electromagnets. The control objective is to ensure accurate valve opening and closing with small contact velocity V_c of all the moving parts. The small contact velocity ($V_c < 0.1$ m/s), also known as "soft landing," is a very important consideration because high contact velocities correlate with noise and component wear [11]. The opening and the closing of the valves have to be achieved within a very small time travel interval ($\delta t_c \approx 3.5$ ms), otherwise engine operation at high speed will deteriorate. These two requirements are obviously conflicting. Other control difficulties arise from 1) the nonlinear characteristics of the actuator; 2) the limited range of actuation and control input saturation; and 3) unknown and varying gas flow forces acting on the valves.

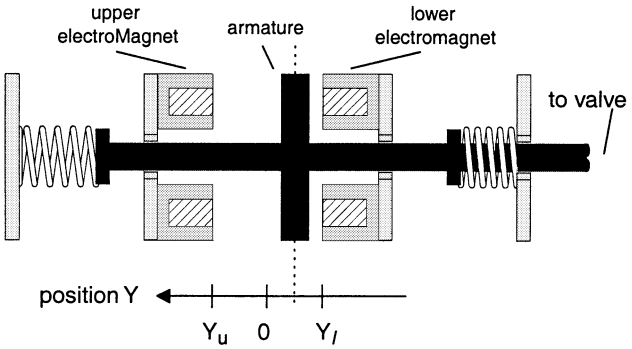

Fig. 1. Electromagnetic actuator of the valve

To address the problem, we design a tracking controller for the valve position Y. The desired valve opening and closing events are generated from the engine management system. The desired trajectory Y_d is designed to be a smooth continuation of the free valve motion. The closed-loop system comprises of a fast inner loop controller and a cycle-to-cycle outer loop controller. In the inner loop, the lower coil voltage U_l is equal to a preset constant voltage $U_l^{\rm pre}$ for large armature-coil gaps, and is the output of a linear feedback stabilizing controller otherwise. The feedback is active only during the last portion of the armature travel because the magnetic force is weak during large gaps. On the other hand, the preset voltage $U_l^{\rm pre}$ to the coils during large gaps allows the flux to build up and prepares a powerful electromagnetic field for when the feedback is switched on. The linear feedback stabilizing controller that drives the armature to a reference constant position is designed based on linearization and discretization of the plant at an the contact point. It is important here to note that the plant is unstable at any equilibrium close to the contact point.

In order to improve the transient behavior of the inner loop controller, an outer controller is designed that calculates the reference Y_r armature position used by the feedback controller as well as the voltage $U_l^{\rm pre}$. Both signals are updated between consecutive cycles (full armature travel) based on the error between the desired position Y_d and the actual position Y by using an iterative

Manuscript received September 11, 2001; revised June 12, 2002. Manuscript received in final form August 12, 2002. Recommended by Associate Editor, K. L. Moore. This work is supported by the National Science Foundation under contract ECS-0049025; matching funds are provided by Ford Motor Company. The work of W. Hoffmann was done while he was with the Department of Mechanical and Environmental Engineering, University of California, Santa Barbara, CA 93106 USA.

W. Hoffmann was with the Department of Mechanical and Environmental Engineering, University of California, Santa Barbara, CA 93106 USA. He is now with Siemens AG, Erlangen, Germany.

K. Peterson and A. Stefanopoulou are with the Department of Mechanical Engineering, University of Michigan, Ann Arbor, MI 48109 USA.

Digital Object Identifier 10.1109/TCST.2003.809242

learning control (ILC) methodology [1], [17]. As a consequence, the corresponding learning algorithm has to calculate more input values than error values. We first present how the ILC approach accounts for a general nonsquare system by introducing decoupling learning algorithms. Then, we parameterize the learning algorithm for the special case based on a linearized model of the plant.

Our first results on a square ILC that only adjusts the reference position Y_r are reported in [5]. The extension to nonsquare ILC in [4] gives good simulation results and show that the landing velocity of the valve is decreasing faster from cycle to cycle if U^{pre} is manipulated by the learning controller. Similarly to our work, the authors in [13] and [14] use stability and convergence condition for repetitive control to the learning (repetitive learning) control problem and achieve small and repeatable contact velocity (average of 0.06 m/s) with a 42-V power supply. However, the actuator has very soft springs that result in a long travel interval (8.0 ms). Note here that a classical repetitive controller is not adequate for this problem since the initial conditions flux, position, and velocity are to be reset at the beginning of each trial (reset after landing and switched to a previously defined "hold" voltage). Also, it is not known before hand when a new opening process will start. The initiation of the valve motion depends on the engine management system through the crankshaft and the driver demand signals, so the reference signal is not periodic.

The authors in [2] mention the use of adaptive control but do not specify which error they used in their cycle adaptation. Finally, the authors in [12] reported the use of adaptation based on the momentum at the middle position only. In general, one-point adaptation entails high sensitivity and low repeatability, especially because of variability due to combustion and noise. Our iterative algorithm forms a weighted error between the desired and the actual valve position sampled every 0.1 ms. The weights are selected using singular value decomposition to achieve fast cycle-to-cycle learning and convergence to the optimum feedforward control signal without large unnecessary corrections that can reduce the system repeatability [4]. Moreover, an ILC does not require an explicit feedforward controller, which parameters are adapted. Investigations regarding the feedforward controller structure and its output range capability in creating a signal that will achieve soft landing can be simplified. In ILC, the commanded reference input is generated directly. As stated in [10], "ILC derives the output of the best possible inverse of the system dynamics." Also, ILC calculates the feedforward signal off-line, whereas, adaptive techniques usually work online, so less computation power is needed.

We show here that soft landing (below 0.05 m/s) can be achieved even under the influence of a varying external force acting on the valve F_v. The profile of the F_v used in the simulations is similar to the one observed in a firing camless engine reported in [15]. In the simulations presented here, the peak force increases 2 N every ten cycles (iterations) to emulate a varying engine load. Experimental results show good tracking performance and a significant reduction of the impact velocity (0.04 m/s) during valve landing after 35 cycles. The average travel interval is 3.9 ms.

This paper is organized as follows. The EMV actuator model and analysis at different equilibria are briefly presented in Sections II and III, respectively. The controller objectives and structure are presented in Section IV. The linear feedback controller design and simulations are shown in Section V. Section VI shows the development of the learning controller. Closed-loop simulations are shown in Section VII, experimental results are shown in Section VIII and concluding remarks are presented in Section IX.

II. Preliminaries and Model

In the sequel, continuous-time variables and their associated signals are denoted by $S(t)$. Their discrete counterparts are denoted by $S[n]$. The variable at an equilibrium point (e.p.) is denoted by S^0, and the deviation between the signal and e.p. is denoted by $s[n] = S[n] - S^0$. The discrete signal of the kth cycle is denoted by $s[n, k]$. And finally, bold face font style, $\boldsymbol{v}$ and $\boldsymbol{M}$, is used for vectors and matrices.

A brief description of the model of the EMV actuator is presented. For detailed analysis and validation of the model see [15]. The actuator consists of a mechanical and an electromagnetic subsystem that can be described by the following variables. The desired and actual armature position is denoted by Y_d and Y and the upper/lower position limit by $Y_u - h/Y_l + h$, where $2 \cdot h$ is the armature thickness [all in meters (m)]. The armature velocity is denoted by V in (m/s), the voltage applied to the upper/lower coil by $U_{u/l}$ in volts (V), the current in the upper/lower coil by $I_{u/l}$ in amps (A), the flux of the upper/lower coil by $\Phi_{u/l}$ in nanometers per amp (Nm/A). The magnetic force is denoted by $F_{u/l}$ in N and the valve force due to pressure F_v in Newtons (N).

The mechanical subsystem can be modeled as a spring–mass–damper system including the external magnetic forces F_u of the upper and F_l of the lower electromagnet and the forces acting on the valve due to the pressure difference between the cylinder and the intake/exhaust runners F_v. A force balance yields

$$m\frac{dV(t)}{dt} = -DY(t) - GV(t) + F_l(t) + F_u(t) + F_v(t) \quad (1)$$

where $m = 0.2$ kg is the mass of the moving parts, $G = 6.0$ kg/s is the friction coefficient, and $D = 150\,000$ kg/s^2 is the spring constant.

The electromagnetic system of the upper and the lower coils is modeled by a resistance/reluctance–circuit

$$U_l(t) = RI_l + \frac{d\Phi_l(t)}{dt} \quad (2)$$

$$U_u(t) = RI_u + \frac{d\Phi_u(t)}{dt} \quad (3)$$

with $R = 50$ in (Ω) being the coil resistance.

The coil currents $I_{l/u}(t)$ are modeled with a nonlinear function f_I of the armature gaps ($Y - Y_l - h$ and $Y_u - Y - h$) and the flux

$$I_l = f_I\left(\Phi_l,\, Y - Y_l - h\right)$$

$$I_u = f_I\left(\Phi_u,\, Y_u - Y - h\right)$$

with

$$f_I\left(\Phi,\, Y\right) = \frac{\Phi}{L_f - \Delta L_f\left(1 - e^{-Y/Y_f}\right)}.$$

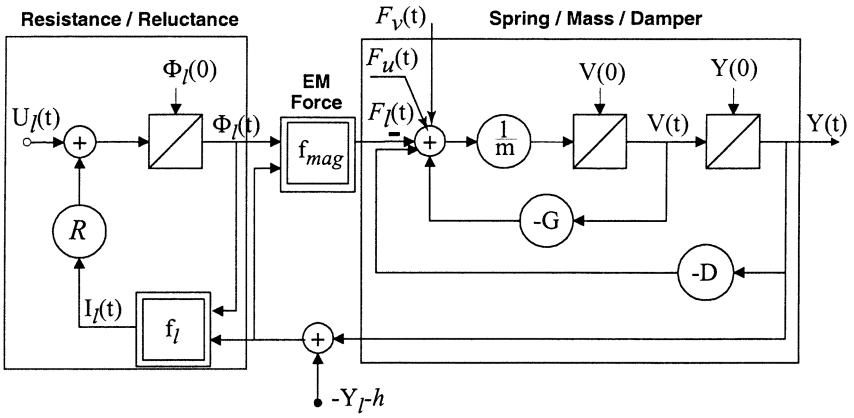

Fig. 2. Block diagram of the EMV actuator model without representation of the upper coil.

The mechanical and electromagnetic subsystems are linked by the magnetic force equations of the two electromagnets

$$F_l = -f_{\text{mag}}\left(\Phi_l,\, Y - Y_l - h\right)$$
$$F_u = f_{\text{mag}}\left(\Phi_u,\, Y_u - Y - h\right).$$

with

$$f_{\text{mag}}\left(\Phi,\, Y\right) = \frac{\Delta L_f \Phi^2 e^{-Y/Y_f}}{2Y_f\left(L_f - \Delta L_f\left[1 - e^{-Y/Y_f}\right]\right)^2}.$$

The distances $Y_l = -4.1$ mm, $Y_u = 4.1$ mm, and $h = 0.1$ mm and the parameters $L_f = 0.06$ Vs/A, $\Delta L_f = 0.027$ Vs/A, and $Y_f = 0.5$ mm are calibrated based on data in [15].

To summarize, the plant has two inputs, upper voltage $U_u(t)$ and lower voltage $U_l(t)$, respectively. The plant output is the armature position $Y(t)$. The four elements of the state vector are position $Y(t)$, velocity $V(t)$, lower flux $\Phi_l(t)$, and the upper flux $\Phi_u(t)$.

Thus, the state–space description of the model is given by

$$\frac{dY}{dt} = V \tag{4}$$
$$\frac{dV}{dt} = -\frac{D}{m}Y - \frac{G}{m}V + \frac{F_u}{m} + \frac{F_l}{m} + \frac{F_v}{m} \tag{5}$$
$$\frac{d\Phi_u}{dt} = -RI_u + U_u \tag{6}$$
$$\frac{d\Phi_l}{dt} = -RI_l + U_l. \tag{7}$$

A block diagram representation of above equations is shown in Fig. 2. The upper coil is not included because of symmetry. Due to the symmetry between the opening and the closing problem, we will concentrate on the opening phase from now on. The model is implemented in Matlab/Simulink.

III. Analysis

The equilibrium points are obtained by solving the state-space equations for $(d/dt)\left[Y(t), V(t), \Phi_l(t), \Phi_u(t)\right] \equiv \mathbf{0}$, and constant inputs. The assumption $U_u(t) \equiv 0$ and $U_l(t) \equiv U_l^0$ yields a stable equilibrium point at $[0,\, 0,\, \Phi_l^0,\, 0]^T$ and an unstable equilibrium point at $[Y^0,\, 0,\, \Phi_l^0,\, 0]^T$. Fig. 3 shows the spring force and the magnetic force for constant flux values

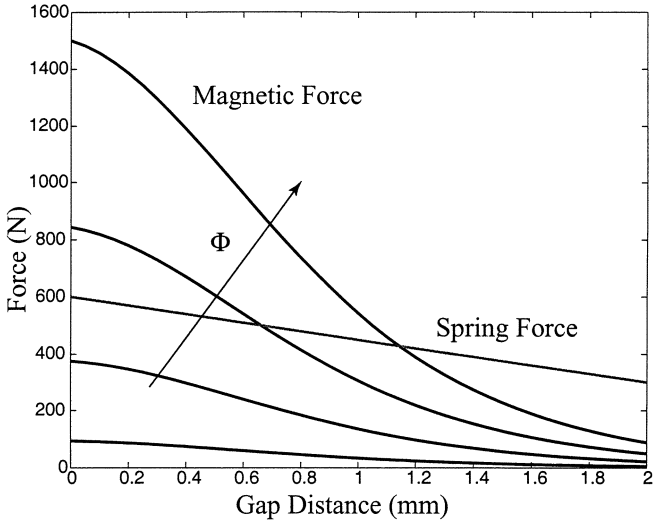

Fig. 3. Force diagram.

during small armature-coil gaps. The equilibrium gap is defined at the intersections of the magnetic force with the spring force when we assume zero valve force $F_v = 0$. The slopes of the two forces are such that a small perturbation will cause the armature to accelerate toward the contact point, or to accelerate toward the stable equilibrium (near the middle position). Fast control of the flux is then required to stabilize the armature. The electromagnetic system dynamics is, however, slow due to the large coil inductance imposing a stringent bandwidth constraint to the control loop.

Apart from the bandwidth limitations, the electromagnetic system has limited control authority. It can be shown that the system cannot be driven into the unstable equilibrium point if $Y^0 \geq -3.25$ mm due to voltage saturation at $U_l^{\max} = 200$ V (Fig. 4). Note also that the magnetic force of the upper coil F_u is approximately zero in equilibrium points $Y^0 \leq -3.25$ mm.

The analysis of the plant is continued by linearizing the state–space equations around one of the above examined unstable equilibrium points. Since the magnetic force of the upper coil F_u is negligible for the unstable equilibrium close to the lower coil, the input $U_u(t)$ and (6) do not have to be considered in the following linearization. The state vector reduces to $[Y(t),\, V(t),\, \Phi_l(t)]^T$.

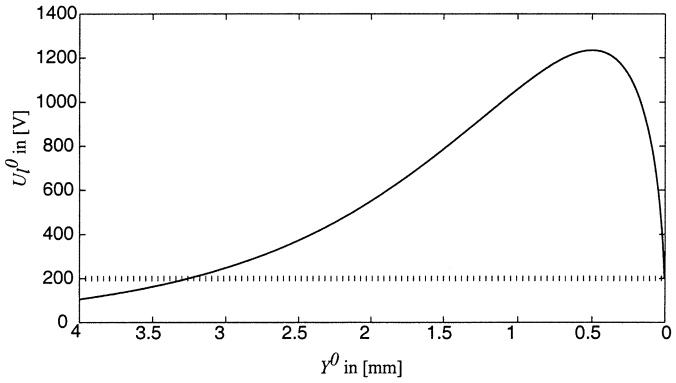

Fig. 4. Voltage in the unstable equilibrium points for various positions. The dotted line corresponds to the maximum voltage of the available source. For $Y^0 = Y_l - h$, the gap is closed.

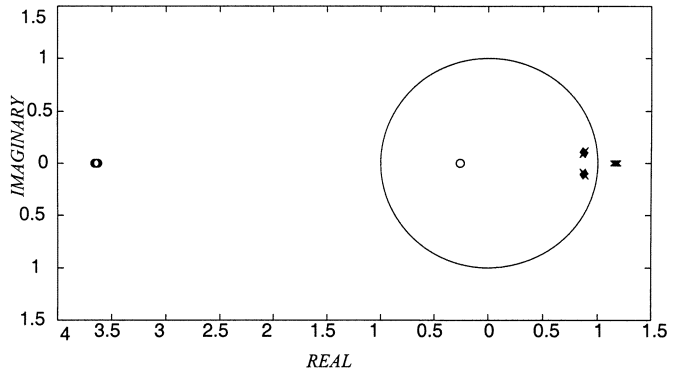

Fig. 5. Zeros and poles loci of the linearized discrete plant in the equilibrium points $Y^0 \in [0,\ 1,\ 2,\ 3,\ 4,\ 5] \cdot 0.1$ mm. The sample time is chosen to be $T_S = 0.1$ ms.

Defining as $\boldsymbol{x} = [y(t),\ v(t),\ \varphi_l(t)]^T$ the deviation from the nominal equilibrium point $[Y^0,\ V^0,\ \Phi^0]$ a linear state–space description

$$\frac{d\boldsymbol{x}}{dt} = \boldsymbol{A}_0\boldsymbol{x} + \boldsymbol{b}_0 u_l$$
$$y = \boldsymbol{c}_0^T\boldsymbol{x}. \tag{8}$$

is derived by linearization of the model equations. The values and units of the elements of A_o, b_o, and c_o are given below

$$\boldsymbol{A}_o = \begin{bmatrix} 0\ (\mathrm{s}^{-1}) & 1 & 0\ (\mathrm{m}/(\mathrm{Vs}^2)) \\ 150\,000\ (\mathrm{s}^{-2}) & -30\ (\mathrm{s}^{-1}) & -47\,434\ (\mathrm{m}/(\mathrm{s}^3\mathrm{V})) \\ -94\,868\ (\mathrm{V/m}) & 0\ (\mathrm{Vs/m}) & -833\ (\mathrm{s}^{-1}) \end{bmatrix}$$

$$\boldsymbol{b}_o = \begin{bmatrix} 0\ (\mathrm{m}/(\mathrm{Vs})) \\ 0\ (\mathrm{m}/(\mathrm{Vs}^2)) \\ 1 \end{bmatrix} \quad \text{and} \quad \boldsymbol{c}_o = \begin{bmatrix} 1 \\ 0\ (\mathrm{s}) \\ 0\ (\mathrm{m}/(\mathrm{Vs})) \end{bmatrix}.$$

The three poles and two zeros of the corresponding discrete transfer–function depend on the equilibrium point. Their locations in the z plane are shown in Fig. 5. The linearized and discretized plant is unstable and nonminimum phase in all the considered equilibrium points.

IV. Controller Structure

Variable valve timing is used to optimize the engine operation with respect to emissions, fuel economy, and drivability. The engine management system typically generates the commands for the initiation of the valve motion (opening or closing) based on the driver's torque demand and other vehicle variables. These commands are not typically periodic during engine acceleration and decelerating conditions which precludes the use of repetitive control. On the other hand, the states of the valve actuator are known and defined at the initiation of motion that suggests the use of ILC for this application.

The "valve travel interval" (δt_c) is defined as the time interval from the beginning of the valve motion to the contact timing t_c, where $Y - (Y_l + h) < 10^{-5}$ m. The corresponding velocity is defined as the contact (or impact) velocity $V_c \stackrel{!}{=} V(t_c)$. The EMCV control system is required to achieve the following two objectives.

- It should reduce the armature-coil and valve-cylinder contact velocities. High contact velocity results in noise and component wear. Engine manufacturers are designing camshafts to achieve a low contact velocity $V_c < 0.1$ m/s.
- It should ensure a small and consistent valve travel interval $\delta t_c \approx 3.5$ ms This requirement ensures that the actuator can open and close the engine valves even during high crankangle speed.

These two objectives are conflicting and, thus, difficult to achieve. Moreover, we need to achieve them independently of unknown forces acting on the valve due to the gas flow. During valve opening events, the gas flow forces can be positive or negative depending on the upstream and downstream valve pressure conditions. To achieve the above two conflicting requirements and avoid use of excessive power and actuation saturation, we design a controller that acts only at the last phase of the valve motion (for feasible equilibrium points). We call t_{fb} the time when $Y_{fb} \stackrel{!}{=} Y(t_{fb}) \leq -3.70$ mm based on the discussion in Section II. The controller achieves tracking of a reference trajectory Y_d with a small travel interval and contact velocity that is a smooth continuation of the initial valve motion $(t < t_{fb})$ with

$$Y_d(t) = (Y_l + h) + (Y_{fb} - (Y_l + h)) \cdot \exp\left(\frac{V_{fb}}{(Y_{fb} - (Y_l + h))}\right)(t - t_{fb}) \tag{9}$$

where Y_{fb} and V_{fb} are the position and velocity of the valve motion during the feedback controller activation.

Fig. 6 shows the controller structure. The armature is assumed to be held by the upper electromagnet in the position $Y_u - h$ and then to be released by disconnecting the upper voltage source at $t = t_0$. As the armature approaches the defined position Y_{fb}, the actuator input signal $U_l[n]$ is switched from $U_l^{\mathrm{pre}}[n]$ to the output of an observer-based feedback controller. The feedback controller is absolutely necessary here because the open-loop actuator dynamics is unstable. Note here that the ILC is a feedforward controller that gets recomputed every cycle and thus cannot alter the open-loop system stability.

In order to improve the transient behavior of the "plant with feedback," a feedforward controller changes its inputs $Y_r[n]$ and $U_l^{\mathrm{pre}}[n]$. The new inputs are calculated by an ILC and updated between consecutive cycles (full armature travel) k and $k+1$. The ILC is processing the error between the desired posi-

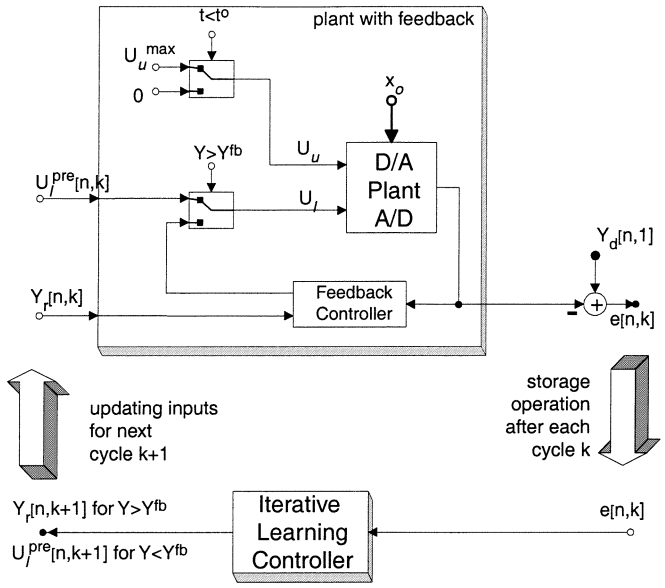

Fig. 6. Controller structure with the inner feedback controller and the outer iterative learning controller.

tion $Y_d[n]$ and the actual position $Y[n,\ k]$. Detailed information about the learning controller is given in Section VI. The Section V discusses the design of the feedback controller.

V. Stabilizing Feedback Controller

The armature is assumed to be held by the upper electromagnet in the position $Y_u - h$ and then to be released by disconnecting the upper voltage source at $t = t_0$. As the armature approaches the defined position Y^{fb}, the plant input signal $U_l(t)$ is switched from a constant previous value $U^{\rm pre}$ to the feedback controller signal. $U^{\rm pre}$ is used to preset the state $\Phi_l(t)$ close to the equilibrium point value Φ^0.

As feedback controller we use a linear-quadratic state-feedback regulator with observer, designed based on a linearization of the plant at the contact point $Y^0 = Y_l + h$. The output feedback is designed to stabilize the unstable armature position dynamics based on the linear quadratic regulator (LQR) methodology. Tuning of the LQR controller gains is a challenging task due to the design requirements of fast transition and zero-overshoot. Note here that any overshoot in the armature response will cause excessive contact velocity and potential bouncing. Beyond the poor performance, bouncing results in discontinuous response which might inhibit the ILC controller from learning and improving the transient system behavior. Additional precaution should be applied when tuning the LQR gains in order to avoid input voltage saturation. After several design iterations the state weight matrix, Q, is selected to be the identity and the actuator weight, r, is one ($Q = I$ and $r = 1$).

The observer poles are set four times faster than the resulting poles of the closed loop system: $(-4453 + 5615j,\ -4453 - 5615j,\ -5452)$. The controller input is never disconnected from the plant in order to reduce observer error. This is a critical feature of our controller. Small velocity and flux estimation error are necessary before the feedback controller activation. Recall that the desired valve trajectory in (9) is implemented using the filtered valve position $\hat{Y}_{fb}$ and estimated velocity $\hat{V}_{fb}$. Finally,

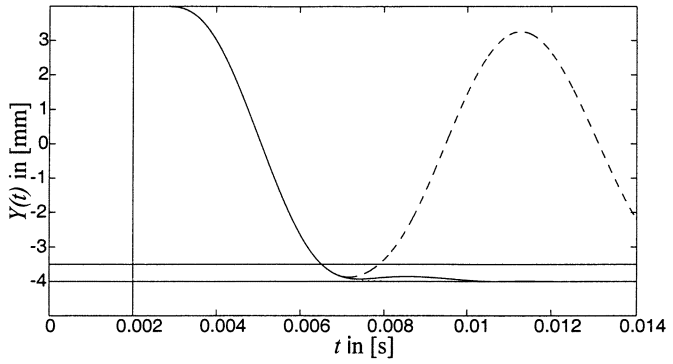

Fig. 7. Position of the armature with (solid) and without (dashed) feedback controller.

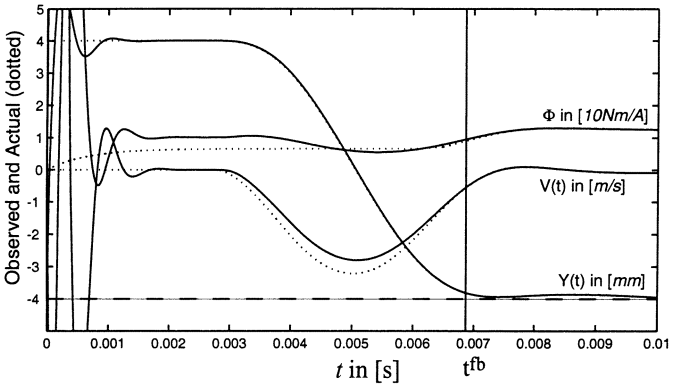

Fig. 8. Observed states (solid) tend to the states (dotted). Transient errors are small at t_{fb}, when the controller is switched on.

a discrete version of the controller is obtained by emulating the resulting controller functions using Tustin's method.

In Fig. 7 the dashed line shows the armature travel for the open-loop system (damped oscillation). The solid line corresponds to the armature travel with the observer-based feedback controller. The detail of the armature travel just before the contact with the lower coil is shown in Fig. 9 (for $k = 1$). Detailed comparison between the observed and the actual states can be seen in Fig. 8. The feedback controller is stabilizing the armature close to the contact point but the transient behavior is rather poor.

VI. Tracking Iterative Learning Controller

In order to achieve better tracking of the desired position, the cyclic character of the process is exploited by use of the ILC introduced in Section IV. In the next two sections, we review the learning control methodology and introduce a class of decoupling learning algorithms.

A. ILC

Let the input and output sequences of a system be $u[n]$ and $y[n]$, respectively. To formulate ILC in a compact way, we need to define the following mapping by defining the operator Γ: $\mathbb{R}^M \mapsto \mathbb{R}^N$ as $\boldsymbol{y} = \Gamma(\boldsymbol{u})$, introducing the vectors

$$\boldsymbol{u} = \begin{bmatrix} u[n] \\ \vdots \\ u[n+M-1] \end{bmatrix} \quad \text{and} \quad \boldsymbol{y} = \begin{bmatrix} y[n+1] \\ \vdots \\ y[n+N] \end{bmatrix}$$

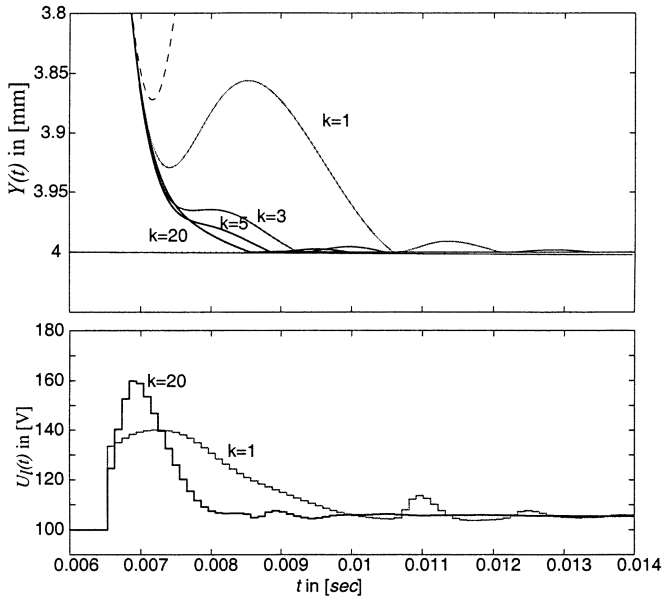

Fig. 9. Positions Y, Y_d and lower voltage U_l for cycles $k = 1, 3, 5, 20$.

where $\boldsymbol{u} \in \mathbb{R}^M$ and $\boldsymbol{y} \in \mathbb{R}^N$. The purpose of the ILC is to find some vector $\boldsymbol{u}^\star$ with the property $\Gamma(\boldsymbol{u}^\star) \cong \boldsymbol{y}_d$, the vector $\boldsymbol{y}_d$ is some desired output vector. If more than one solution exists, $\boldsymbol{u}^\star$ is supposed to have the smallest L_2–Norm of all the solutions. In order to solve this problem, the cyclic characteristic of the process is exploited. Let the cycles be numbered with k. In the first cycle, the input vector $\boldsymbol{u}[1]$ is applied to the system. This vector and the corresponding output vector $\boldsymbol{y}[1]$ are used to generate an improved input vector $\boldsymbol{u}[2]$ for the next cycle, and so forth. Thus, a linear formulation of the ILC algorithm reads as

$$\boldsymbol{u}[k+1] = \boldsymbol{S}\boldsymbol{u}[k] + \boldsymbol{E}(\boldsymbol{y}_d - \boldsymbol{y}[k]) \tag{10}$$

where the matrices $\boldsymbol{S} \in \mathbb{R}^{M\times M}$ and $\boldsymbol{E} \in \mathbb{R}^{M\times N}$ weight the previous input $\boldsymbol{u}[k]$ and the previous error $\boldsymbol{e}[k] = \boldsymbol{y}_d - \boldsymbol{y}[k]$, respectively. They have to be chosen in a way that the sequence $\{\boldsymbol{u}[k]\}$ converges in the sense of the L_2–norm to

$$\boldsymbol{u}^\star = \lim_{k\to\infty} \boldsymbol{u}[k]. \tag{11}$$

B. Decoupling Learning Controllers

The class of decoupling learning controllers is now derived by linearizing the discrete process Γ at the equilibrium point, yielding a matrix $\boldsymbol{P} \in \mathbb{R}^{N\times M}$ with the property $\boldsymbol{y} = \Gamma(\boldsymbol{u}) \cong \boldsymbol{P}\boldsymbol{u}$. The entries of $\boldsymbol{P}$ will be discussed later. In the following, we assume $M \geq N$, as we need this case later. To derive the decoupling learning controller, we apply the SVD to the matrix $\boldsymbol{P}$, yielding $\boldsymbol{P} = \boldsymbol{L}\boldsymbol{\Lambda}_P\boldsymbol{R}^T$, where $\boldsymbol{R} \in \mathbb{R}^{M\times M}$ and $\boldsymbol{L} \in \mathbb{R}^{N\times N}$ are orthonormal matrices. General information about svd can be found in [3]. The matrix $\boldsymbol{\Lambda}_P \in \mathbb{R}^{N\times M}$ has the singular values $\sigma_0 > \sigma_i > 0\ \forall\ \in [0, N-1]$ in its main diagonal, all other entries are zero. The largest singular value σ_0 is the L_2–norm of $\boldsymbol{P}$. Let for simplicity, $\boldsymbol{\Lambda}_P = [\boldsymbol{\Sigma}|\boldsymbol{0}]$, where $\boldsymbol{\Sigma}$ is a square matrix with all the nonzero singular values of $\boldsymbol{\Lambda}_P$ in its diagonal.

We define decoupling learning algorithms by setting $\boldsymbol{S} = \boldsymbol{R}\boldsymbol{\Lambda}_S\boldsymbol{R}^T$ and $\boldsymbol{E} = \boldsymbol{R}\boldsymbol{\Lambda}_E\boldsymbol{L}^T$, where $\boldsymbol{\Lambda}_S \in \mathbb{R}^{M\times M}$ is a diagonal matrix with the entries $s_0, \ldots, s_{M-1}$, and $\boldsymbol{\Lambda}_E \in \mathbb{R}^{M\times N}$ is a diagonal matrix with the entries $e_0, \ldots, e_{N-1}$ on its main diagonal. Using (10) for analysis the linear model equation $\boldsymbol{y} = \boldsymbol{P}\boldsymbol{u}$ instead of $\boldsymbol{y} = \Gamma(\boldsymbol{u})$, we get

$$\boldsymbol{u}[k+1] = \boldsymbol{S}\boldsymbol{u}[k] + \boldsymbol{E}(\boldsymbol{y}_d - \boldsymbol{P}\boldsymbol{u}[k]). \tag{12}$$

Using above equations, we can write (12) in the form

$$\boldsymbol{R}^T\boldsymbol{u}[k+1] = (\boldsymbol{\Lambda}_S - \boldsymbol{\Lambda}_E\boldsymbol{\Lambda}_P)\boldsymbol{R}^T\boldsymbol{u}[k] + \boldsymbol{\Lambda}_E\boldsymbol{L}^T\boldsymbol{y}_d.$$

Defining the transformed vectors $\boldsymbol{\nu}[k] = \boldsymbol{R}^T\boldsymbol{u}[k]$ and $\boldsymbol{\mu} = \boldsymbol{L}^T\boldsymbol{y}_d$, we get

$$\boldsymbol{\nu}[k+1] = \left[\begin{array}{ccc|c} s_0 - e_0\sigma_0 & & & \\ & \ddots & & \boldsymbol{0} \\ & & s_{\overline{N}} - e_{\overline{N}}\sigma_{\overline{N}} & \\ \hline & & & s_N \\ \boldsymbol{0} & & & \ddots \\ & & & s_{M-1} \end{array}\right] \boldsymbol{\nu}[k] + \left[\begin{array}{c} e_0 \\ \ddots \\ e_{\overline{N}} \\ \hline \boldsymbol{0} \end{array}\right] \boldsymbol{\mu} \tag{13}$$

with $\overline{N} = N - 1$. The above choice of $\boldsymbol{E}$ and $\boldsymbol{S}$ obviously yields decoupling of the learning law (12). Thus, to determine the convergence properties of the learning controller only the scalar equations

$$\nu_i[k+1] = (s_i - e_i\sigma_i)\nu_i[k] + e_i\mu_i \quad \forall i \in [0, N-1] \tag{14}$$

$$\nu_i[k+1] = s_i\nu_i[k] \quad \forall i \in [N, M-1] \tag{15}$$

have to be studied instead of a matrix equation. Equation (15) converges for $|s_i| < 1$ to $\nu_i^\star = 0$. That means all components of the input vector that do not affect the valve position (pointing into the null-space of the linearized plant) are learned to be zero. Solving the recursive (14) yields

$$\nu_i[k] = (s_i - e_i\sigma_i)^k\nu_i[0] + \frac{1-(s_i - e_i\sigma_i)^k}{1 - s_i - e_i\sigma_i}\, e_i\mu_i \qquad \forall i \in [0, N-1] \tag{16}$$

which converges to

$$\nu_i^\star = \frac{e_i}{1 - s_i - e_i\sigma_i}\,\mu_i \quad \text{for } |s_i - e_i\sigma_i| < 1.$$

Generally, the e_i the s_i's of $\boldsymbol{\Lambda}_E$ and $\boldsymbol{\Lambda}_S$, respectively, must be chosen to ensure that the convergence condition $|s_i - e_i\sigma_i| < 1$ holds true. Examples for decoupling laws are in [7], where they choose the transposed system matrix $\boldsymbol{E} = (1/c)\,\boldsymbol{P}^T (= (1/c)\,\boldsymbol{R}\boldsymbol{\Lambda}_P^T\boldsymbol{L}^T)$. In other words, the e_i's are (implicitly) chosen to be $e_i = (\sigma_i/c)$ ($c \geq \sigma_0^2$ must hold to ensure convergence). Another example of decoupling learning law can be found in [9], where a pseudoinverse approach $\boldsymbol{E} = \boldsymbol{P}^\# (= \boldsymbol{R}\boldsymbol{\Lambda}_P^\#\boldsymbol{L}^T)$ yields $e_i = \sigma_i^{-1}$ for $\sigma_i \neq 0$.

We have chosen $\boldsymbol{E} = (1/\sigma_0)\,\boldsymbol{R}\boldsymbol{L}^T$ [the same as $e_i = (1/\sigma_0)$] because in the EMV actuator application, this yields good simulation results. The learning velocity is faster than in the transposed matrix approach. Compared with the pseudoinverse ap-

proach, high values of $e_i = \sigma_i^{-1}$ (in the case of small singular values) are also avoided. The M elements s_i of $\mathbf{\Lambda}_S$ are chosen to be $s_i = 1\ \forall i \in [0,\ N-1]$ and $s_i = 0\ \forall i \in [N,\ M-1]$. This choice ensures zero output error. In addition, of all input vectors that cause zero error, the ones with the smallest norm are learned.

To summarize, in this paper, (14) and (15) are parameterized by $s_i = 1$, $e_i = (1/\sigma_0)\ \forall i \in [0,\ N-1]$ and $s_i = 0\ \forall i \in [N,\ M-1]$. This choice results in

$$\nu_i[k+1] = \left(1 - \frac{\sigma_i}{\sigma_0}\right)\nu_i[k] + \frac{1}{\sigma_0}\mu_i \to \frac{1}{\sigma_i}\mu_i \quad \forall i \in [0,\ N-1]$$

$$\nu_i[k+1] = s_i\nu_i[k] = 0 \quad \forall i \in [N,\ M-1]$$

and, therefore

$$\boldsymbol{\nu}^\star = \lim_{k\to\infty}\boldsymbol{\nu}[k] = \begin{bmatrix}\mathbf{\Sigma}^{-1}\\ \mathbf{0}\end{bmatrix}\boldsymbol{L}^T\boldsymbol{y}_d. \tag{17}$$

Thus, the zero input directions are learned to zero. For all other input directions the convergence speed is determined by $1 - \sigma_i/\sigma_0$. On the other hand, the steady-state ν_i^∞ is proportional to σ_i^{-1}. Therefore, output components, that require lower input signals are learned faster than components requiring higher input signals. This is a useful feature regarding input saturations or nonminimum phase systems. In the general case and returning to the original coordinates, we get

$$\boldsymbol{u}^\star = \boldsymbol{R}\boldsymbol{\nu}^\star = \boldsymbol{R}\begin{bmatrix}\mathbf{\Sigma}^{-1}\\ \mathbf{0}\end{bmatrix}\boldsymbol{L}^T\boldsymbol{y}_d \tag{18}$$

which involves the pseudoinverse of the matrix $\boldsymbol{P} = \boldsymbol{L}[\mathbf{\Sigma}|\mathbf{0}]\boldsymbol{R}^T$.

C. EMV Input–Output Mapping

In the EMCV actuator problem every cycle k the ILC will shape $M-N$ values of the preset voltage $U_l^{pre}[n,\ k]$ and the N reference trajectory values $Y_r[n,\ k]$ that are applied as a reference command to the observer-based closed-loop system when it becomes active ($Y[n,\ k] \le Y_{fb}$). We employ the lowercase notation, i.e., variables are defined as the deviation between the signal and equilibrium point.

The input vector $\boldsymbol{u}$ of Section VI-A comprises in this paper of a sequence of the lower voltage u_l and a sequence of the reference position y_r

$$\boldsymbol{u} = \begin{bmatrix} u_l[n_{fb} - M + N]\\ \vdots\\ u_l[n_{fb}-1]\\ y_r[n_{fb}]\\ \vdots\\ y_r[n_{fb}+N-1]\end{bmatrix} \stackrel{!}{=} \begin{bmatrix}\boldsymbol{u}_l\\ \boldsymbol{y}_r\end{bmatrix} \in \mathbb{R}^M.$$

Thus, $M-N$ values of the lower voltage and N values of the desired position will be learned. As far as the plant output is concerned, the position $y[n]$ is considered after switching on the feedback controller, therefore

$$\boldsymbol{y} = [\,y[n_{fb}+1]\cdots y[n_{fb}+N]\,]^T$$

defines the vector $\boldsymbol{y}$ introduced in Section VI-A. The measurements that the ILC will use to learn in the next iteration depend on 1) the response of the electromagnetic system due to the initial condition after the application of the preset voltage and 2) the output response of the observer-based closed-loop EMCV actuator. Specifically, two effects contribute to $\boldsymbol{y}$.

- The output $\boldsymbol{y}^\varphi$ of the closed-loop system due to the voltage that has been applied to the lower electromagnet before switching on the observer-based feedback. This voltage causes a certain value of the lower flux φ_l^{fb} (state variable) at the moment of switching.
- The output $\boldsymbol{y}^{y_r}$ of the closed-loop system due to its input y_d after switching.

Linearizing the mapping between $\boldsymbol{u}$ and $\boldsymbol{y}$ yields the matrix $\boldsymbol{P}$ of Section VI-B. Let this matrix be composed of two matrices $\boldsymbol{P}^\varphi \in \mathbb{R}^{N\times M-N}$ and $\boldsymbol{P}^{y_r} \in \mathbb{R}^{N\times N}$ defined by

$$\boldsymbol{y}^\varphi + \boldsymbol{y}^{y_r} = \underbrace{[\boldsymbol{P}^\varphi|\boldsymbol{P}^{y_r}]}_{\boldsymbol{P}}\begin{bmatrix}\boldsymbol{u}_l\\ \boldsymbol{y}_r\end{bmatrix}. \tag{19}$$

In order to derive $\boldsymbol{P}^\varphi$, the value φ_l^{fb} of the lower flux at the moment of switching must be determined. This is done using a simplification of the linearized model in Fig. 2, precisely by neglecting the influence of the position Y on the lower flux. Neglecting the variability of the reluctance on the armature gap allows us estimate easily φ_l^{fb}. The assumed constant value of the reluctance is chosen to be the averaged reluctance value observed during the valve traveling before Y_{fb}. Assuming a constant reluctance yields a simple resistance–reluctance circuit with the transfer function $(\varphi_l(s)/u_l(s)) = (T_r/sT_r + 1)$ with $T_r = (L_f + 0.5\,\Delta L_f/R)$. $h_\varphi[n]$ is the impulse response of the discrete version of this transferfunction using a zero-order hold. Thus, the lower flux at the switching instant is given by

$$\varphi_l^{fb} = [h_\varphi[M-N],\ \ldots,\ h_\varphi[1]]\cdot\boldsymbol{u}_l \stackrel{!}{=} \boldsymbol{h}_\varphi^T\cdot\boldsymbol{u}_l. \tag{20}$$

A linear model describing the influence of the state φ_l^{fb} on the plant output is

$$\boldsymbol{y}^\varphi = \boldsymbol{p}^\varphi\cdot\varphi_l^{fb} \tag{21}$$

where $\boldsymbol{p}^\varphi \in \mathbb{R}^N$ is determined by simulation. Equations (19) and (20) yield

$$\boldsymbol{P}^\varphi = \boldsymbol{p}^\varphi\cdot\boldsymbol{h}_\varphi^T. \tag{22}$$

The matrix $\boldsymbol{P}^{y_r}$ is a typical convolution matrix of the input-output observer-based closed-loop EMCV actuator behavior. Its entries are the elements of the impulse response sequence of the linearized discretized closed-loop system.

VII. Simulation Results

Simulation results for the case of zero gas flow force are presented first in Fig. 9. These results are similar to the one shownd in our previous work [5] where the preset voltage was not modified by the ILC. In Fig. 9 (bottom plot) one can observe a small

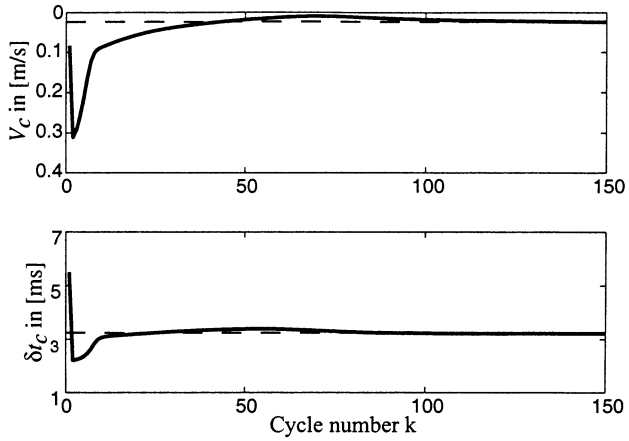

Fig. 10. Travel interval and contact velocity during learning in the case without F_{gas}. The desired trajectory has $V_c = -0.023\,(m/s)$ and $\delta t_c = 3.25$ ms.

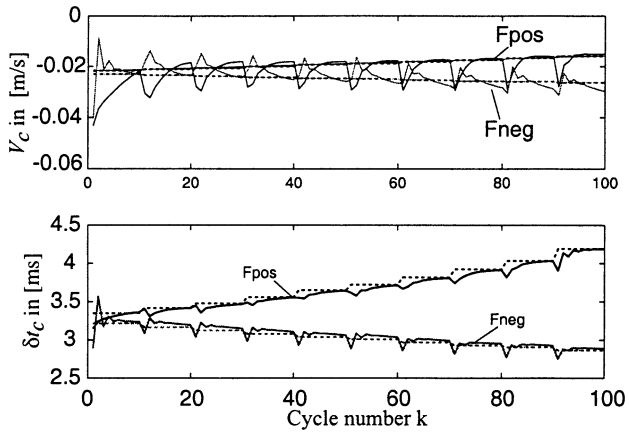

Fig. 11. Desired (dashed) and achieved (solid) impact velocity and travel time for positive F_v and negative F_v.

drop in the preset voltage just before the activation of the feedback loop. Fig. 10 demonstrates the achieved contact velocity and the associated travel interval for each cycle.

Fig. 11 shows that the impact velocity and the travel interval in the case where there is an unknown varying valve force applied in the valve. This force is the result of the difference between the upstream and downstream pressure on the poppet valve. Experimental data in [15] show that a realistic valve force during valve opening will have its absolute maximum value F_v^p at the beginning of the valve motion $Y = Y_u - h$ and it decreases to zero as the valve reaches its minimum value $Y = Y_l + h$. In the simulations shown in Fig. 11, we increase the absolute maximum value F_v^p by 2 N every ten cycles to allow gradual learning. We consider conditions where the gas force opposes the valve opening motion (positive F_v) and vice versa (negative F_v). The positive gas force corresponds to conditions observed during exhaust valve opening against high cylinder pressure. Negative gas force corresponds to conditions during a late intake valve opening (for zero valve overlap). The achieved impact velocities are well bellow the desired value 0.1 m/s. Note here that the impact velocity for the positive F_v is gradually reduced despite the increasing positive peak gas forces. This is accompanied with an associated increase in the travel interval shown in

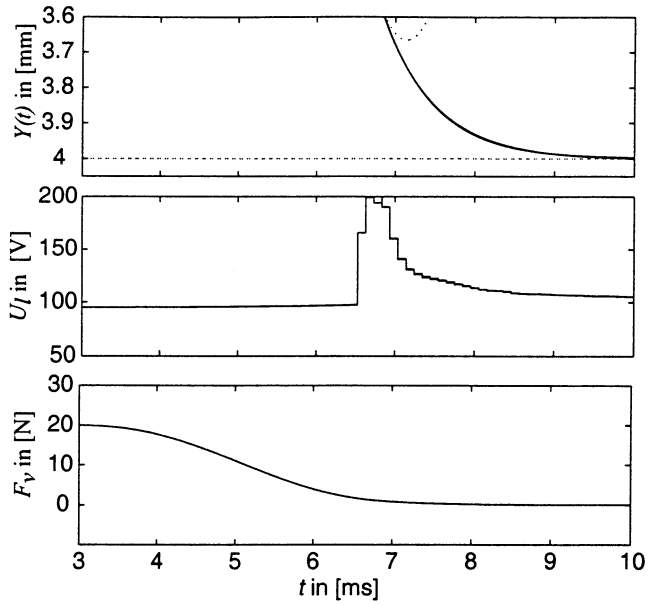

Fig. 12. Position Y, Y_d, lower voltage U_l and disturbance F_v during learning. Each subplot shows the cycles $k = 92, 94, 96, 98, 100$.

the bottom plot. Due to the increasing peak gas force, the feedback switches on later (t_{fb} increases) and the switching velocity value V_{fb} decreases. Both these effects result in a varying valve desired trajectory $Y_d[n]$. The impact velocity and travel interval of the desired valve trajectory are shown in Fig. 11 together with the achieved one. Note here that a long travel interval is allowable during the valve opening phase because the flow is insensitive to the valve lift during large lift values ($Y \approx Y_l + h$).

Figs. 12 and 13 show the detailed valve trajectory, coil voltage, and gas force during several selected cycles. The gas force applied in the valve is shown in the bottom plot in both figures. In particular, Fig. 12 emulates conditions where the gas force opposes the valve opening motion, whereas, Fig. 13 demonstrates the negative gas force case.

In the case of negative F_v, the values of $U_l^{pre}[n]$ are learned to lower values than in the case of $F_v = 0$, see Fig. 9 (bottom). This results in a lower magnetic force $F_l(t)$, which compensates the effect of $F_v(t)$, see (1). In the case of a large opposing gas force, the preset voltage value needs to be adjusted to higher values to ensure that the valve fully opens and the lower coil catches the armature. Iterative adjustment of the preset voltage values using the above explained learning algorithm provides the efficiency and robustness needed.

VIII. Experimental Results

The ILC is implemented on the EMV actuator using the experimental configuration shown in Fig. 14. The experiment consists of the following components: an electromechanical valve actuator, an eddy current sensor, two pulsewidth-modulated (PWM) drivers, one 200-V power supply, and a Dspace 1103 processing board. The Eddy current sensor is on the rear of the actuator and measures the displacement of a target disc that is mounted as an extension of the armature. Thus, the Eddy current sensor measurement is sampled by the Dspace processor at 20 kHz. Based on the displacement measurement

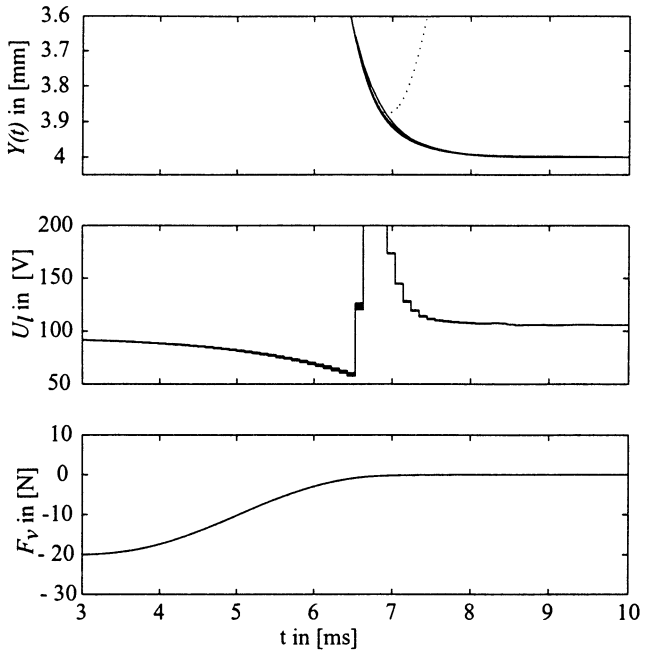

Fig. 13. Position Y, Y_d, lower voltage U_l and disturbance F_v during learning. Each subplot shows the cycles $k = 92, 94, 96, 98, 100$.

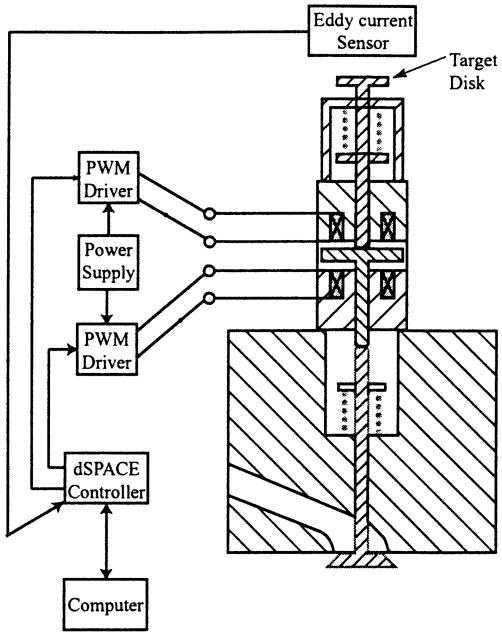

Fig. 14. Experimental setup.

and the control algorithm described above (observer-based feedback + ILC), the Dspace processing board regulates the PWM frequency to each of the PWM drivers to achieve the desired performance. The mean noise amplitude in the measured displacement is 0.09 mm while in the fully open position (when the target disk is the farthest away from the Eddy current sensor) and 0.06 mm in the fully closed position. The measurement noise varies almost linearly between these two values as the target disk moves between the two extreme positions.

Due to the limited memory and processing capability of the Dspace 1103 processing board, the ILC algorithm needs to be

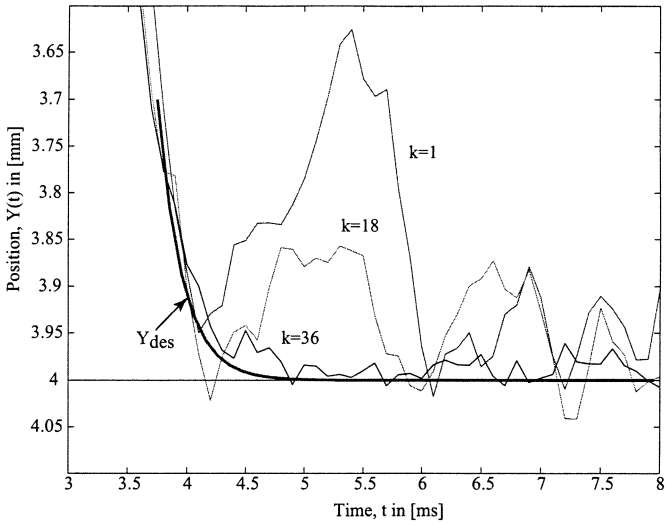

Fig. 15. Desired position Y_d and measured position Y for cycles $k = 1, 18, 36$

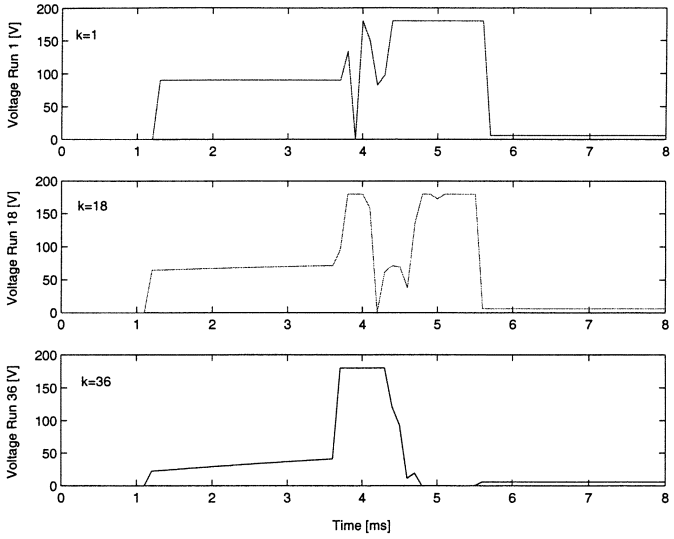

Fig. 16. Voltage command for cycles $k = 1, 18, 36$.

carefully encoded to enable it to run in real time. Thus, the matrix/vector multiplication required in the ILC algorithm is divided up over several time steps. At each time step, the algorithm carries out a single term by term operation. We implemented the ILC algorithm to update the feedforward commands through the opening transition of the valve only. The cyclic valve motion is initiated every 0.8 s.

The tracking performance is demonstrated in Fig. 15 that shows the desired position Y_d and measured position Y for cycles $k = 1, 18, 36$. Note that the comparison between the measured and desired position starts just 0.3 mm away from the contact point as indicated by the beginning of the desired position trajectory Y_d.

The voltage command for the three cycles is shown in Fig. 16. Note that the first part of the voltage command $U_l^{\text{pre}}[n, k]$ is modified by the ILC algorithm designed in Section VI-B, whereas, the last part is defined by the observer-based feedback controller designed in Section V. The transition to the closed-loop voltage command is noticeable at approximately

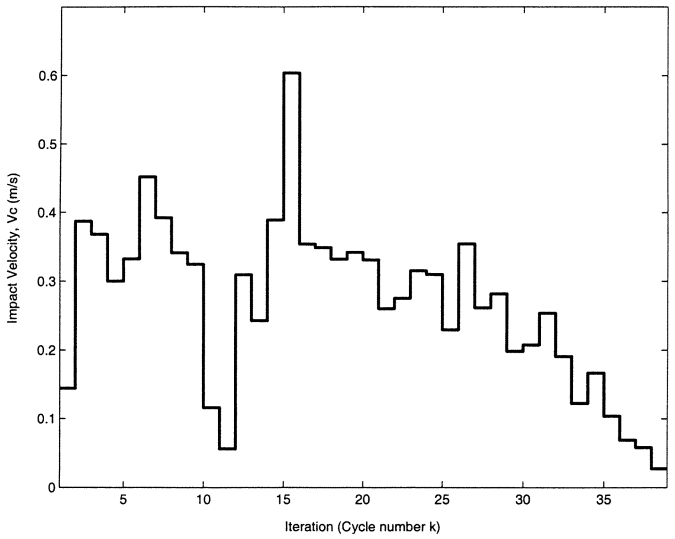

Fig. 17. Impact velocity during learning.

3.6 ms, or more precisely, when the position is 0.3 mm away from the contact point. During the last part of the motion, the ILC algorithm updates the reference trajectory $Y_r[n, k]$ that is fed to the closed-loop controller reducing the tracking error between the desired Y_d and measured Y position.

The average travel interval achieved through out the experiments is $\delta t_s = 3.9$ ms with maximum $\delta t_s = 4.1$ ms, minimum $\delta t_s = 3.7$ ms, and standard deviation 0.09 ms. The achieved travel interval is slightly longer than the desired valve travel interval and the one shown in the simulations of Fig. 17 for zero gas force. Further experiments and discussions with Ford and Volvo engineers indicated that the actuator friction coefficient and the actuator mass is higher than the desired one due to the addition of the target disk for the Eddy current sensor. This modification decreased the damped frequency of the spring-mass-damper system and contributed to the longer travel interval.

Small contact velocities ($V_c < 0.1$ m/s) are achieved after 35 iterations as shown in Fig. 17. The contact velocity decreases monotonically after 15 iterations despite the initial transients in the ILC controller that cause large contact velocities. Although we cannot store and, consequently plot, the system performance for long run periods, we report here that low contact velocity of 0.04 m/s can be maintained.

IX. Conclusion

In this paper, we introduce and formulate the control problem and the requirements for small contact velocity (soft landing) and travel interval of an EMV actuator used in camless engines. We, then design a feedback and a feedforward iterative learning controller and demonstrate through simulation good performance during nominal conditions and uncertain "engine firing" conditions. The algorithm is implemented on a benchtop experimental setup. Experimental results show consistent contact velocity of 0.04 m/s and travel interval of 3.9 ms.

The next step is to validate the control design on an experimental engine. Few difficulties will arise during implementation. In particular, the valve/armature separation, also known as "valve lash" will require modifications both in the desired trajectory and the feedback controller design. Nevertheless, the ILC control methodology designed here has substantial potential as a practical solution to the soft landing problem in camless engine valvetrains with far-reaching consequences in future internal combustion engine design.

Acknowledgment

The authors thank M. Haghgooie, T. Megli, and Y. Wang from Ford Motor Company and R. Otterspeer from Volvo Cars for lending us the valve actuator and advising us throughout the project. They thank G. McNey from the University of California, Santa Barbara, for the eddy current sensor development. They also thank L. Paden from Magnetic Moments, Goleta, CA, for her help in fabricating the eddy current sensor and the donation of its signal processing unit.

References

[1] S. Arimoto, S. Kawamura, and F. Miyazaki, "Bettering operation of robots by learning," *J. Robot. Syst.*, vol. 1, no. 2, pp. 123–140, 1984.

[2] S. Butzmann, J. Melbert, and A. Koch, "Sensorless control of electromagnetic actuator for variable valve train,", SAE Paper 2000-01-1225, 1999.

[3] H. G. Golub and C. F. van Loan, *Matrix Computations*. Baltimore, MD: Johns Hopkins Univ. Press, 1983.

[4] W. Hoffmann and A. G. Stefanopoulou, "Iterative learning control of electromechanical camless valve actuator," in *Proc. Amer. Contr. Conf.*, June 2001, pp. 2860–2866.

[5] ——, "Valve position tracking for soft landing of electromechanical camless valvetrain," in *Proc. IFAC Workshop Automotive Contr.*, Karlsruhe, Germany, Mar. 2001, pp. 305–310.

[6] W. C. Kim, I. S. Chin, K. S. Lee, and J. Choi, "Analysis and reduced order design of quadratic criterion-based iterative learning control using singular value decomposition," *Comput. Chem. Eng.*, vol. 25, pp. 1815–1819, 2000.

[7] G. Lee-Glauser, J.-N. Juang, and R. W. Longman, "Comparison and combination of learning controllers: Computational enhancement and experiments," *J. Guidance, Contr. Dyn.*, vol. 19, no. 5, pp. 1116–1123, 1996.

[8] R. B. Mathews, "Electromagnetic Control Device," U.S. Patent 2 769 943, Aug. 22, 1949.

[9] K. L. Moore, "Iterative learning control of determenistic systems," in *Advances in Industrial Control*. New York: Springer-Verlag, 1993.

[10] ——, "Iterative learning control—An Expository Overview," *Appl. Comput. Contr., Signal Processing, Circuits*, pp. 151–214, 1999.

[11] D. J. Podnar, "Development of an electromagnetic valve actuation system on a Kohler engine,", Final Interim Rep., DARPA Contract DAAK70-92-C-0059, Mar. 1998.

[12] V. F. Schultz and W. E. Seitz, *Gently Does It*: press release of Venture Scientifics, LLC, 1997.

[13] C. Tai, A. Stubbs, and T. C. Tsao, "Modeling and controller design of an electromagnetic engine valve," in *Proc. Amer. Contr. Conf.*, June 2001, pp. 2890–2895.

[14] C. Tai and T. C. Tsao, "Quiet seating control design of an electromagnetic engine valve actuator," in *Proc. 2001 ASME Int. Mech. Eng. Congr. Expos.*, IMECE2001/DSC-24 520.

[15] Y. Wang, A. Stefanopoulou, M. Haghgooie, I. Kolmanovsky, and M. Hammoud, "Modeling of an electromechanical valve actuator for a camless engine," in *Proc. 5th Int. Symp. Advanced Vehicle Contr.*, Aug. 2000.

[16] Y. Wang, "Camless valvetrain: Control challenges and techniques," Ph.D. dissertation, Univ. California, Santa Barbara, 2001.

[17] J.-X. Xu and Z. Bien, "The frontiers of iterative learning control," in *Iterative Learning Control*, Z. Bien and J.-X. Xu, Eds. Boston, MA: Kluwer, 1998, pp. 9–35.

Wolfgang Hoffmann received the Dipl. Ing. degree in electrical engineering from the University of Erlangen-Nuremberg, Erlangen, Germany, in 1995 and is currently pursuing the Ph.D. degree at the same university.

In 1996, he joined Siemens AG, Automation and Drives, Erlangen. In 2000, he was Visiting Researcher at the Center for Control Engineering and Computation, University of California, Santa Barbara. Since 2001, he has been with Siemens AG, Transportation Systems, Erlangen. His research interests include inverter drives, electromagnetic compatibility, and control applications.

Katherine Peterson received the Bachelor's degree in mechanical engineering from the University of Illinois, Urbana, in May 2000. Currently, she is working toward the Ph.D. degree in mechanical engineering at the University of Michigan, Ann Arbor.

In Summer 2001 and 2002 she worked as a summer intern in Ford Research Laboratorys, Detroit, MI. Her research focuses on the design and development of nonlinear and linear learning controllers for electromechanical actuators.

Anna G. Stefanopoulou received the Diploma degree in 1991 from the National Technical University of Athens, Greece, the M.S. degree in Naval Architecture and Marine Engineering in 1992 from the University of Michigan, Ann Arbor, and the M.S. and Ph.D. degrees in the University of Michigan, Electrical Engineering and Computer Science department, in 1994 and 1996, respectively.

She was an Assistant Professor at the University of California, Santa Barbara, and a Technical Specialist at the Ford Research Laboratory, Detroit, MI. She is presently an Associate Professor at the Mechanical Engineering Department at the University of Michigan. She holds five U.S. patents. Her current research interests are in control of breathing through valves, vanes and membranes, control of internal combustion engines, and fuel cell power systems.

Dr. Stefanopoulou is Chair of the Transportation Panel in ASME DSCD and an Associate Editor of the IEEE TRANSACTIONS ON CONTROL SYSTEM TECHNOLOGY. She is a recipient of a 2002 Ralph Teetor SAE Educational Award, a 1997 NSF CAREER, and a 1999 UCSB SPUR Undergraduate Research Mentor Award. She was selected as one of the top young innovators from the 2002 Technology Review (TR100), and she was an invitee of the 1999 and 2001 National Academy of Engineering Symposium on Frontiers of Engineering.